

**České vysoké učení technické v Praze, Fakulta
stavební**

**Czech Technical University in Prague, Faculty
of Civil Engineering**

Ing. Jan Zeman, Ph.D.

**Homogenizace heterogenních materiálů s
náhodnou geometrií**

**Homogenization of Heterogeneous Materials
with Random Geometry**

Summary

In the last two decades, the theory of heterogeneous materials has made a significant process from mainly theoretical discipline to an applicable engineering tool. Major advances have been achieved in the field of modelling material systems with deterministic properties of individual constituents and widely separated lengthscales. Nevertheless, most real-world materials display random features, both in the intrinsic material properties as well as due to limited information on the mutual arrangement of phases. Moreover, the assumption of separated lengthscales may often be a limiting factor, especially when addressing systems with localized response. Therefore, the focus of this lecture is on heterogeneous material systems without clearly defined hierarchy of lengthscales and with geometry distribution specified in terms of the second-order spatial statistics.

The methods investigated include a representative of perturbation methods, the Karhunen-Loève expansion technique coupled with the Monte-Carlo simulation and a solver based on the Hashin-Shtrikman variational principles. In all cases, parameters of the underlying random field of material properties are directly derived from image analysis of a real-world structure. Added value as well as limitations of individual schemes are illustrated by a case study of an irregular historical masonry panel.

Souhrn

Teorie heterogenních materiálů v posledních dvou desetiletích prošla bouřlivým rozvojem od převážně teoretické disciplíny až k aplikovatelnému inženýrskému nástroji. Hlavního pokroku bylo dosaženo v oboru modelování materiálových systémů s deterministickými vlastnostmi složek a jasně oddělenými měřítky. Většina inženýrských materiálů nicméně vykazuje náhodné chování, a to jak v materiálových datech tak i kvůli omezené informaci o uspořádání jednotlivých složek. Navíc může předpoklad oddělených měřítek představovat zásadní omezení, a to především při zkoumání systémů s lokalizovanou odezvou. Proto je tato přednáška zaměřena na heterogenní materiálové systémy bez jasně definované hierarchie délkových měřítek a s geometrií specifikovanou pouze pomocí prostorové statistiky druhého řádu.

Prezentované metody zahrnují reprezentanta perturbačních metod, techniku Karhunen-Loèveho rozvoje spojenou se simulací Monte-Carlo a řešič založený na Hashin-Shtrikmanových variačních principech. Ve všech případech jsou parametry náhodného pole materiálových vlastností přímo odvozeny z obrazové analýzy skutečné konstrukce. Přidaná hodnota stejně jako omezení jednotlivých schémat jsou ilustrovány pomocí pilotní studie nepravidelného historického zdiva.

Klíčová slova

náhodné heterogenní materiály; stochastická homogenizace; dvojbodová statistika; vylepšená perturbační metoda; Karhunen-Loèveho rozvoj; Hashin-Shtrikmanovy variační principy

Keywords

random heterogenous materials; stochastic homogenization; two-point statistics; improved perturbation methods; Karhunen-Loève expansion; Hashin-Shtrikman variational principles

České vysoké učení technické v Praze

Název: Homogenizace heterogenních materiálů s náhodnou geometrií
Autor: Ing. Jan Zeman, Ph.D.
Počet stran: 24
Náklad: 150 výtisků

© Jan Zeman, 2009
ISBN:

Contents

1	Introduction	6
2	Quantification of random geometry	7
3	Improved perturbation method	10
4	Karhunen-Loève expansion	11
5	Hashin-Shtrikman variational principles	14
6	Numerical example	17
7	Conclusions	19

1 Introduction

Analysis of material with heterogeneous microstructure is a fascinating subject with far-reaching applications in virtually all areas of applied sciences and engineering. In essence, the implicit assumption adopted in the majority of the heterogeneous media-oriented studies is that on the lowest relevant scale of resolution, the behavior of individual constituents is relatively easy to characterize in terms of universal intrinsic properties, whereas the intricately complex response seen in the macroscopic world can be rationally deduced from field equations of continuum physics, supplemented with an appropriate scale-bridging scheme and eventually with the stochastic aspects of the problem at hand. The foundations of this research programme were established in the sixties of the last century by Hill and, since then, the field has witnessed a rapid development, resulting in a thorough understanding of engineering, physical, numerical and mathematical aspects of the problem.

In general, it can be stated that the dominant mechanisms governing the response of heterogeneous media are well-understood when fulfilling the assumptions of

- *separation of scales* hypothesis, which requires the characteristic dimensions of the heterogeneous microstructure on individual levels of resolution as well as the characteristic wavelength of the fields involved to be widely separated,
- *deterministic* description of geometry of individual constituents.

This claim can be fully justified by rapidly increasing applications of the homogenization principles to wide range of civil engineering materials such as wood [9], cement paste [21], masonry [12], or even to complex historical structures [23]; see also [20] for an up-to-date review.

Nevertheless, most real-world materials display random features, both in the intrinsic material properties as well as due to limited information on the mutual arrangement of phases. Moreover, the assumption of separated lengthscales may appear to be a limiting factor, especially when addressing systems with localized response. Therefore, the focus of this lecture is on heterogeneous material systems without clearly defined hierarchy of lengthscales and with geometry distribution specified in terms of the second-order spatial statistics.

In particular, three numerical approaches to the determination of the overall response of heterogeneous media with comparable macro-

and meso-lengthscales are presented. A unifying feature is the description of mechanical properties in the form of a random field with the second-order statistics consistently derived from image analysis of the investigated structure. In Section 2, this procedure is briefly summarized following the exposition of Falsone and Lombardo [5]. The second level of representation involves the determination of basic statistics related to the response of a finite size heterogeneous masonry structure. In particular, the improved perturbation method is introduced first in Section 3, followed in Section 4 by the Monte-Carlo approach with individual realizations of the random field generated using the Karhunen-Loève expansion. Section 5 is concerned with the application of the Hashin-Shtrikman variational principles, coupled with the Finite Element discretization to allow for the treatment of finite-size bodies. In Section 6, the results obtained with the selected methods are mutually compared on the basis of elastic analysis of an irregular masonry panel. Finally, Section 7 introduces possible extensions and refinements of the studied approaches.

2 Quantification of random geometry

Before getting to the heart of the matter, we begin by summarizing essential terminology related to the theory of random fields [19]. Given a complete probability space $\{\Theta, \mathcal{F}, \mathcal{P}\}$ with sample space Θ , σ -algebra \mathcal{F} on Θ and probability measure \mathcal{P} on \mathcal{F} , a scalar random field H defined on an open set $\Omega \subset \mathbb{R}^d$ is a mapping

$$H : \Theta \times \Omega \rightarrow \mathbb{R}, \quad (1)$$

such that, for every $x \in \Omega$, $H(x; \theta)$ is a random variable with respect to the triple $\{\Theta, \mathcal{F}, \mathcal{P}\}$. The mean of a random field is then given as

$$\mu_H(x) = \mathbb{E} [H(x; \theta)] = \int_{\Theta} H(x; \theta) d\mathcal{P}(\theta), \quad (2)$$

for any $x \in \Omega$, whereas the covariance of two random fields H and G is defined by

$$R_{HG}(x, x') = \mathbb{E} [(H(x; \theta) - \mu_H(x)) (G(x'; \theta) - \mu_G(x'))], \quad (3)$$

with the symbol $R_H(x, x') = R_{HH}(x, x')$ reserved for the autocovariance, reducing to a variance for $x = x'$:

$$\sigma_H^2(x) = \mathbb{E} [(H(x; \theta) - \mu_H(x))^2]. \quad (4)$$

A random field $H(\mathbf{x}; \theta)$ is said to be homogeneous if all its joint probability distribution functions (PDFs) remain invariant under the translation of the coordinate system, leading to substantial simplification of the considered statistics. Finally, assuming that the autocovariance function can be well-approximated by an exponential function, the correlation length λ_H is defined by means of inequality:

$$\forall \|\mathbf{x} - \mathbf{x}'\| \geq \lambda_H : R_H(\mathbf{x} - \mathbf{x}') \leq \frac{\sigma_H^2}{\exp(1)}, \quad (5)$$

hence quantifying the characteristic dimension of the spatial fluctuations. Finally, a random field is ergodic if all information on joint PDFs are available from a single realization of the field.

Of particular importance is the characteristic function related to the spatial distribution of the i -th phase:

$$\chi^{(i)}(\mathbf{x}; \theta) = \begin{cases} 1 & \text{if } \mathbf{x} \in \Omega^{(i)}(\theta), \\ 0 & \text{otherwise,} \end{cases} \quad (6)$$

where $\Omega^{(i)}(\theta)$ is the domain occupied by the i -th phase for realization θ and i can take values $\{s, m\}$, where s denotes the stone phase and m refers to the mortar phase. The characteristic functions of individual phases are not independent, once e.g. the ‘‘stone’’ characteristic function is provided, the complementary descriptor follows from

$$\chi^{(m)}(\mathbf{x}; \theta) + \chi^{(s)}(\mathbf{x}; \theta) = 1. \quad (7)$$

Therefore, we concentrate on the stone phase in the sequel.

When assuming the statistically uniform and ergodic media, the basic spatial statistics is provided by

$$\mu_{\chi^{(s)}} = c^{(s)}, \quad R_{\chi^{(s)}}(\mathbf{x} - \mathbf{x}') = S_2^{(s)}(\mathbf{x} - \mathbf{x}') - \left(c^{(s)}\right)^2, \quad (8)$$

where $c^{(s)}$ is the volume fraction of the relevant phase and $S_2^{(s)}$ coincides with the two-point probability function, defined for generic phases $i, j \in \{s, m\}$ as [18]

$$S_2^{(ij)}(\mathbf{x}, \mathbf{x}') = \mathbb{E} \left[\chi^{(i)}(\mathbf{x}; \theta) \chi^{(j)}(\mathbf{x}'; \theta) \right], \quad (9)$$

hence quantifying the probability of two points \mathbf{x} and \mathbf{x}' being located in phases i and j (with $S_2^{(ii)}$ abbreviating $S_2^{(ii)}$).

The statistical descriptors of real mesostructures can be evaluated on the basis of a digitized images of the investigated sample. Under the periodic boundary condition, the statistics can be efficiently evaluated using the Fast Fourier transform techniques; see e.g. [6]. To automate the acquisition of these functions, a software working in **MATLAB** was implemented [5], covering all the basic steps of mesostructure quantification with the data provided in the form of a color image, see Figure 1 for an illustration of the procedure.

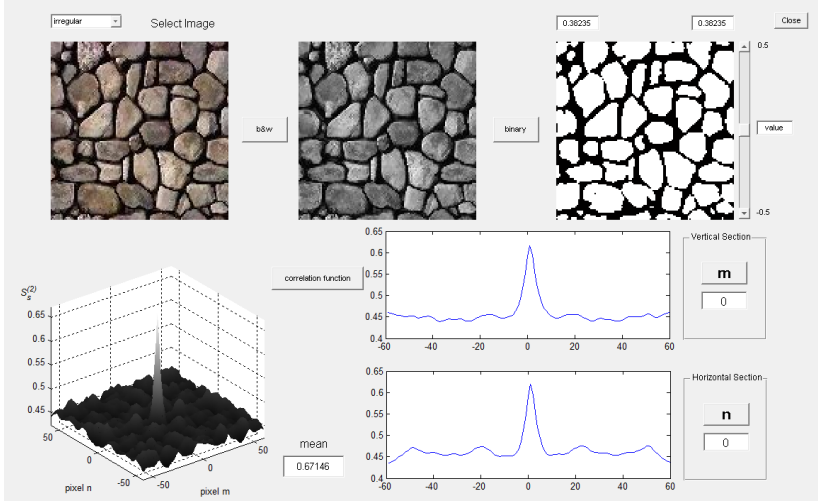


Figure 1: Example of the program used to obtain correlation function for a chaotic masonry panel (San Marco d'Alunzio, Italy).

The phase characteristic functions allow us to directly express the matrix-valued field of material properties in the form

$$\mathbf{C}(\mathbf{x}; \theta) = \chi^{(s)}(\mathbf{x}; \theta) \mathbf{C}^{(s)} + \chi^{(m)}(\mathbf{x}; \theta) \mathbf{C}^{(m)}, \quad (10)$$

where $\mathbf{C}^{(s)}$ and $\mathbf{C}^{(m)}$ are the deterministic material stiffness matrices of the two constituents. The mean and the covariance functions then follow from Equations (2) and (3):

$$\mu_{C_{ij}}(\mathbf{x}) = C_{ij}^{(m)} + c^{(s)}(C_{ij}^{(s)} - C_{ij}^{(m)}), \quad (11)$$

$$R_{C_{ij}C_{kl}}(\mathbf{x} - \mathbf{x}') = R_{\chi^{(s)}}(\mathbf{x} - \mathbf{x}') \left(C_{ij}^{(s)} - C_{ij}^{(m)} \right) \left(C_{kl}^{(s)} - C_{kl}^{(m)} \right) \quad (12)$$

see [5] for additional discussion.

3 Improved perturbation method

Consider a mechanical system with the randomness in material properties specified in terms of the random field $\chi^{(s)}(\mathbf{x}; \theta)$. In the context of finite element analysis of static problems, the discretized form of equilibrium equations reads [2]

$$\mathbf{K}_h(\chi^{(s)}(\mathbf{x}; \theta))\mathbf{u}_h(\theta) = \mathbf{F}_h, \quad (13)$$

where h is a characteristic element size, the force vector \mathbf{F}_h is assumed to be deterministic and the global stiffness matrix \mathbf{K}_h is stochastic due to uncertainty in the material properties.

The widely used mid-point method is employed to represent the random field consistently with the underlying finite element mesh. Therefore, two different considerations control the size of an element h , cf. [1]. In addition to the deterministic requirement, the distance between two adjacent random variables has to be short enough to capture the essential features of the random field. The general recommendation is to choose $2h \approx \lambda_{\chi^{(s)}}$ to describe the stochastic field with sufficient accuracy [14].

In the current implementation, the value at the element center is used to characterize the stochastic field, thus yielding a representation in the form of a vector of random variables

$$\boldsymbol{\chi}_h^{(s)}(\theta) = \left[\chi_{h,1}^{(s)}(\theta) \quad \chi_{h,2}^{(s)}(\theta) \quad \dots \quad \chi_{h,N_e}^{(s)}(\theta) \right]^\top, \quad (14)$$

with $\chi_{h,e}^{(s)}(\theta)$ being the value of $\chi^{(s)}(\mathbf{x}; \theta)$ at the e -th element centroid and N_e denoting the number of elements. The element stiffness matrix is calculated from the standard finite element methodology and is expressed as [2]

$$\mathbf{K}_{h,e} \left(\chi_{h,e}^{(s)}(\theta) \right) = \int_{\Omega_e} \mathbf{B}_{h,e}^\top(\mathbf{x}) \mathbf{C}_e \left(\chi_{h,e}^{(s)}(\theta) \right) \mathbf{B}_{h,e}(\mathbf{x}) \, d\mathbf{x}, \quad (15)$$

where $\mathbf{B}_{h,e}$ is the deterministic displacement-to-strain matrix related to the e -th element and the element material stiffness matrix \mathbf{C}_e follows from Eq. (10). After the assembly procedure, the global form of equilibrium equations becomes

$$\mathbf{K}_h(\boldsymbol{\chi}_h^{(s)}(\theta))\mathbf{u}_h(\theta) = \mathbf{F}_h. \quad (16)$$

Among the various perturbative SFE approaches proposed in literature, an improved perturbation technique proposed in [4] is employed in this work. When compared to the traditional first-order expansion schemes, the added value of the adopted method is that the

mean value of the response variables depends on the covariance information on uncertain input parameters, thereby optimally utilizing the available second-order statistics. Following this approach, the mean of the response vector \mathbf{u}_h is given by

$$\boldsymbol{\mu}_{\mathbf{u}_h} = \mathbf{A}_h^{-1} \mathbf{F}_h, \quad (17)$$

where

$$\mathbf{A}_h = \mathbf{K}_{h,0} - \sum_{i=1}^{N_e} \sum_{j=1}^{N_e} R_{\chi_i^{(s)} \chi_j^{(s)}} \mathbf{K}'_{h,i} \left(\mathbf{K}_{h,0}^{-1} \right) \mathbf{K}'_{h,j}, \quad (18)$$

with the stiffness matrix sensitivities provided by

$$\mathbf{K}_{h,0} = \mathbf{K}_h(\boldsymbol{\chi}_h^{(s)}) \Big|_{\boldsymbol{\chi}_h^{(s)} = \mathbb{E}[\boldsymbol{\chi}_h^{(s)}]}, \quad \mathbf{K}'_{h,i} = \frac{\partial \mathbf{K}_h(\boldsymbol{\chi}_h^{(s)})}{\partial \chi_{h,i}^{(s)}} \Big|_{\boldsymbol{\chi}_h^{(s)} = \mathbb{E}[\boldsymbol{\chi}_h^{(s)}]}. \quad (19)$$

In addition, the autocovariance matrix of displacements follows from

$$\mathbf{R}_{\mathbf{u}_h} = \mathbf{K}_{0,h}^{-1} \mathbf{C}_h \mathbf{K}_{0,h}^{-1}, \quad (20)$$

where

$$\mathbf{C}_h = \sum_{i=1}^{N_e} \sum_{j=1}^{N_e} R_{\chi_i^{(s)} \chi_j^{(s)}} \mathbf{K}'_{h,i} \boldsymbol{\mu}_{\mathbf{u}_h} \left(\boldsymbol{\mu}_{\mathbf{u}_h} \right)^\top \mathbf{K}'_{h,j}, \quad (21)$$

see [4] for additional details.

4 Karhunen-Loève expansion

With reference to the mesostructure-based random fields considered in the current work, we start from the KLE of the characteristic function $\chi^{(s)}(\mathbf{x}; \theta)$ in the form

$$\chi^{(s)}(\mathbf{x}; \theta) = \mu_{\chi^{(s)}}(\mathbf{x}) + \sum_{i=1}^{\infty} \sqrt{\lambda_i} \xi_i(\theta) f_i(\mathbf{x}), \quad (22)$$

where λ_i and $f_i(\mathbf{x})$ are the eigenvalues (decreasing in magnitude) and eigenfunctions of the autocovariance $R_{\chi^{(s)}}(\mathbf{x}, \mathbf{x}')$, $\{\xi_i(\theta)\}$ is a set of random variables [17]. Since the kernel $R_{\chi^{(s)}}(\mathbf{x}, \mathbf{x}')$ is bounded, symmetric and non-negative, it has all eigenfunctions mutually orthogonal and forming a complete set spanning the function space to which

$\chi^{(s)}(\mathbf{x}; \theta)$ belongs. Therefore, the autocovariance function can be decomposed into

$$R_{\chi^{(s)}}(\mathbf{x}, \mathbf{x}') = \sum_{i=1}^{\infty} \lambda_i f_i(\mathbf{x}) f_i(\mathbf{x}'), \quad (23)$$

with eigenfunctions $f_i(\mathbf{x})$ and eigenvalues λ_i found as the solutions of the homogeneous Fredholm integral equation of the second kind

$$\int_{\Omega} R_{\chi^{(s)}}(\mathbf{x}, \mathbf{x}') f_i(\mathbf{x}') d\mathbf{x}' = \lambda_i f_i(\mathbf{x}). \quad (24)$$

The parameter $\xi_i(\theta)$ in Eq. (22) corresponds to an uncorrelated standardized random variable expressed as

$$\xi_i(\theta) = \frac{1}{\sqrt{\lambda_i}} \int_{\Omega} [\chi^{(s)}(\mathbf{x}; \theta) - \mu_{\chi^{(s)}}(\mathbf{x})] f_i(\mathbf{x}) d\mathbf{x}. \quad (25)$$

In practical implementations, the series (22) and (23) are truncated after M terms, yielding the approximations

$$\chi^{(s)}(\mathbf{x}; \theta) \approx \mu_{\chi^{(s)}}(\mathbf{x}) + \sum_{i=1}^M \sqrt{\lambda_i} \xi_i(\theta) f_i(\mathbf{x}), \quad (26)$$

$$R_{\chi^{(s)}}(\mathbf{x}, \mathbf{x}') \approx \sum_{i=1}^M \lambda_i f_i(\mathbf{x}) f_i(\mathbf{x}'). \quad (27)$$

A careful convergence study of truncated KLE presented in [10] has demonstrated, for specific classes of stochastic fields, the dependence of the optimal value of M on the ratio of the characteristic domain length L to the correlation parameter $\lambda_{\chi^{(s)}}$. For weakly correlated processes ($\lambda_{\chi^{(s)}}/L \ll 1$), the higher order eigenvalues cannot be neglected without having a serious impact on the accuracy of the simulation.

Such behavior is illustrated by means of Figure 2, showing the decay of eigenvalues of KLE with the covariance kernel determined for the masonry sample presented in Section 2. In addition, several associated eigenfunctions are collected in Figure 3. Clearly, the random field under consideration is weakly correlated as $\lambda_{\chi^{(s)}}/L \approx 10/120$, see Figure 1, and a large number of terms ($M \approx 200$) is needed to capture fine features of the covariance, cf. Figure 3(d).

With a KLE of the spatial autocovariance function at hand, the individual realizations of the heterogeneous body can be efficiently generated once an appropriate model for the random field $\chi^{(s)}(\mathbf{x}; \theta)$ is

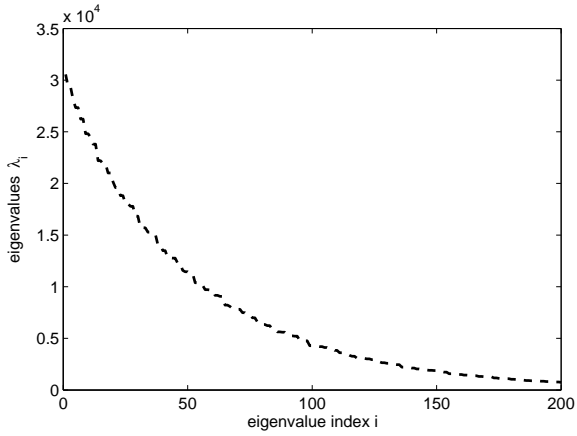


Figure 2: Distribution of eigenvalues for KLE related to chaotic masonry sample.

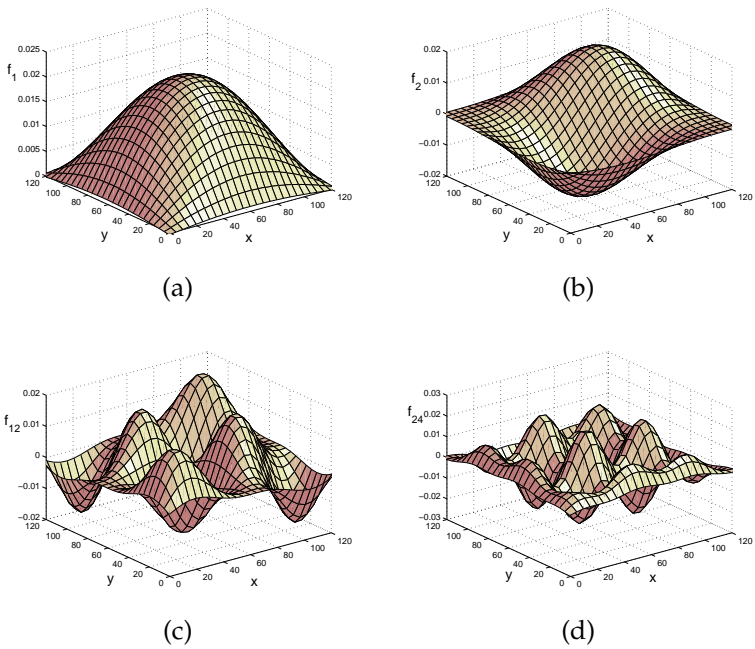


Figure 3: Examples of eigenfunctions f_i ; (a) $i = 1$, (b) $i = 2$, (c) $i = 12$, (d) $i = 24$.

adopted. In the current study, we assume that the random field is Gaussian, for which the coefficients $\xi_i(\theta)$ in Eq. (25) become independent standard Gaussian variables of zero mean and unit variance.

The final step of the KLE-based solver involves the determination of the response statistics for a structure with material stiffness determined from Eq. (10):

$$\mathbf{C}(\mathbf{x}; \theta) \approx \mathbf{C}^{(m)} + \left(c^{(s)} + \sum_{i=1}^M \sqrt{\lambda_i} \xi_i(\theta) f_i(\mathbf{x}) \right) (\mathbf{C}^{(s)} - \mathbf{C}^{(m)}). \quad (28)$$

The frequently adopted framework of spectral SFE [7], where the response variable is discretized using the polynomial chaos expansion in the stochastic coordinate, is not applicable in the current case as the high number of KLE terms results in unmanageable number of polynomial chaos components. Therefore, a simple Monte-Carlo approach is adopted in the present study.

Once the sampling phase is completed, the unbiased mean and covariance of displacement vectors are provided by

$$\boldsymbol{\mu}_{\mathbf{u}_h} = \frac{1}{n} \sum_{j=1}^n \mathbf{u}_h(\theta_j), \quad (29)$$

$$\mathbf{R}_{\mathbf{u}_h} = \frac{1}{n-1} \sum_{j=1}^n \left[\mathbf{u}_h(\theta_j) (\mathbf{u}_h(\theta_j))^{\top} - n \boldsymbol{\mu}_{\mathbf{u}_h} (\boldsymbol{\mu}_{\mathbf{u}_h})^{\top} \right], \quad (30)$$

where n denotes the number of simulations and θ_j is used to denote the j -th deterministic realization.

5 Hashin-Shtrikman variational principles

The last approach investigated here builds on the classical Hashin-Shtrikman variational principles for the heterogeneous media [8], extended to the stochastic setting by Willis [22]. The basic idea of the method is the introduction of a reference homogeneous body with stiffness tensor \mathbf{C}_0 , employed in the analysis instead of an inhomogeneous realization $\mathbf{C}(\mathbf{x}; \theta)$, recall Eq. (10). The heterogeneity of the material is compensated using the polarization stress $\boldsymbol{\tau}(\mathbf{x}; \theta)$, resulting from the stress equivalence condition:

$$\boldsymbol{\sigma}(\mathbf{x}; \theta) = \mathbf{C}(\mathbf{x}; \theta) \boldsymbol{\varepsilon}(\mathbf{x}; \theta) = \mathbf{C}_0 \boldsymbol{\varepsilon}(\mathbf{x}; \theta) + \boldsymbol{\tau}(\mathbf{x}; \theta), \quad (31)$$

with σ and ε denoting the configuration-dependent stress and strain fields. The additional unknown follows from stationarity conditions

$$(\mathbf{u}(\mathbf{x};\theta), \boldsymbol{\tau}(\mathbf{x};\theta)) = \arg \min_{\mathbf{v}(\mathbf{x})} \operatorname{stat}_{\boldsymbol{\omega}(\mathbf{x})} \Pi_{\text{HS}}(\mathbf{v}(\mathbf{x}), \boldsymbol{\omega}(\mathbf{x});\theta) \quad (32)$$

where Π_{HS} stands for the Hashin-Shtrikman (HS) energy functional

$$\begin{aligned} \Pi_{\text{HS}}(\mathbf{v}, \boldsymbol{\omega};\theta) &= \frac{1}{2} \int_{\Omega} \boldsymbol{\varepsilon}^{\top}(\mathbf{v}(\mathbf{x})) \mathbf{C}_0 \boldsymbol{\varepsilon}(\mathbf{v}(\mathbf{x})) \, d\mathbf{x} - \int_{\Omega} \mathbf{v}^{\top}(\mathbf{x}) \mathbf{f}(\mathbf{x}) \, d\mathbf{x} \\ &\quad - \int_{\Gamma_t} \mathbf{v}^{\top}(\mathbf{x}) \mathbf{t}(\mathbf{x}) \, d\mathbf{x} + \int_{\Omega} \boldsymbol{\varepsilon}^{\top}(\mathbf{v}(\mathbf{x})) \boldsymbol{\omega}(\mathbf{x}) \, d\mathbf{x} \\ &\quad - \frac{1}{2} \int_{\Omega} \boldsymbol{\omega}^{\top}(\mathbf{x}) [\mathbf{C}(\mathbf{x};\theta) - \mathbf{C}_0]^{-1} \boldsymbol{\omega}(\mathbf{x}) \, d\mathbf{x}. \end{aligned} \quad (33)$$

In Eq. (32), \mathbf{v} and $\boldsymbol{\omega}$ denote trial values of displacement field and polarization stresses, while $\mathbf{f}(\mathbf{x})$ are deterministic body forces and $\mathbf{t}(\mathbf{x})$ boundary tractions acting on Γ_t , respectively, cf. [13].

The elementary statistics of displacements and polarizations associated with probability density $\mathcal{P}(\theta)$ follow directly from a stochastic variant of Eq. (32):

$$(\boldsymbol{\mu}_u, \boldsymbol{\mu}_\tau) = \int_{\Theta} \left(\arg \min_{\mathbf{v}(\mathbf{x};\theta)} \operatorname{stat}_{\boldsymbol{\omega}(\mathbf{x};\theta)} \Pi_{\text{HS}}(\mathbf{v}(\mathbf{x};\theta), \boldsymbol{\omega}(\mathbf{x};\theta);\theta) \right) \, d\mathcal{P}(\theta). \quad (34)$$

Following the approach of Willis [22], the previous problem is solved approximately by considering the following ansatz for displacements and polarizations:

$$\mathbf{u}(\mathbf{x}, \theta) = \mathbf{u}_0(\mathbf{x}) + \mathbf{u}_1(\mathbf{x};\theta), \quad (35)$$

$$\boldsymbol{\tau}(\mathbf{x};\theta) \approx \chi^{(s)}(\mathbf{x};\theta) \boldsymbol{\tau}^{(s)}(\mathbf{x}) + \chi^{(m)}(\mathbf{x};\theta) \boldsymbol{\tau}^{(m)}(\mathbf{x}), \quad (36)$$

where \mathbf{u}_0 is the deterministic displacement of the reference body subject to distributed body forces and tractions, \mathbf{u}_1 stores the configuration-dependent displacement due to the polarization stress expressed using a non-local operator Γ_0 , cf. Eq. (38) bellow,

$$\mathbf{u}_1(\mathbf{x};\theta) = - \int_{\Omega} \Gamma_0(\mathbf{x}, \mathbf{x}') \boldsymbol{\tau}(\mathbf{x}';\theta) \, d\mathbf{x}', \quad (37)$$

and $\boldsymbol{\tau}^{(i)}$ denotes the deterministic value of the polarization stress related to the i -th phase.

Two levels of approximation are generally needed to fully discretize the problem (34). The first step involves discretizing the Γ_0 operator

together with the “reference” strain distribution, which in the context of the adopted Finite Element approximation become [13]

$$\Gamma_0(\mathbf{x}, \mathbf{x}') \approx \mathbf{B}_h^u(\mathbf{x}) \mathbf{K}_{h,0}^{-1} \mathbf{B}_h^{u\top}(\mathbf{x}'), \quad \boldsymbol{\varepsilon}(\mathbf{u}_0(\mathbf{x})) \approx \mathbf{B}_h^u(\mathbf{x}) \mathbf{u}_{0,h}, \quad (38)$$

where, in analogy with Section 3, $\mathbf{K}_{h,0}$ denotes the stiffness matrix of the reference structure, \mathbf{N}_h^u is the matrix of shape functions and $\mathbf{B}_h = \partial \mathbf{N}_h^u$ is the displacement-to-strain matrix and $\mathbf{u}_{0,h}$ stands for nodal displacement vector determined for the reference problem [2]. In the second step, phase polarization fields are parameterized in the form, cf. [13]

$$\boldsymbol{\tau}^{(i)}(\mathbf{x}) \approx \mathbf{N}_h^\tau(\mathbf{x}) \mathbf{d}_h^{(i)}, \quad (39)$$

where \mathbf{N}_h^τ is the matrix of shape functions to approximate the polarization stresses.

Employing the approximations (38) and (39), the discretized stationary conditions of problem (34) become:

$$\mathbf{K}_h^{(i)} \mathbf{d}_h^{(i)} + \sum_j \mathbf{K}_h^{(ij)} \mathbf{d}_h^{(j)} = \mathbf{R}_h^{(i)}, \quad (40)$$

with the individual terms provided by

$$\mathbf{K}_h^{(i)} = \int_{\Omega} \mathbf{N}_h^\tau \mathbf{T}(\mathbf{x}) c^{(i)} [\mathbf{C}^{(i)} - \mathbf{C}_0]^{-1} \mathbf{N}_h^\tau(\mathbf{x}) \, d\mathbf{x}, \quad (41)$$

$$\mathbf{K}_h^{(ij)} = \int_{\Omega} \int_{\Omega} \mathbf{N}_h^\tau \mathbf{T}(\mathbf{x}) S_2^{(ij)}(\mathbf{x} - \mathbf{x}') \Gamma_{0,h}(\mathbf{x}, \mathbf{x}') \mathbf{N}_h^\tau(\mathbf{x}') \, d\mathbf{x} \, d\mathbf{x}', \quad (42)$$

$$\mathbf{R}_h^{(i)} = \int_{\Omega} \mathbf{N}_h^\tau \mathbf{T}(\mathbf{x}) c^{(i)} \mathbf{B}_h^u(\mathbf{x}) \mathbf{u}_{0,h} \, d\mathbf{x}. \quad (43)$$

Once the degrees of freedom related to the phase polarization stresses are determined from system (40), the mean of displacement value becomes [13]

$$\boldsymbol{\mu}_{u_h}(\mathbf{x}) = \mathbf{N}_h^u(\mathbf{x}) \left(\mathbf{u}_{0,h} - \mathbf{K}_{0,h}^{-1} \int_{\Omega} \mathbf{B}_h^{u\top}(\mathbf{x}') \boldsymbol{\mu}_{\tau_h}(\mathbf{x}') \, d\mathbf{x}' \right), \quad (44)$$

with

$$\boldsymbol{\mu}_{\tau_h}(\mathbf{x}') = \mathbf{N}_h^\tau(\mathbf{x}') \left(c^{(m)} \mathbf{d}_h^{(m)} + c^{(s)} \mathbf{d}_h^{(s)} \right). \quad (45)$$

In addition to the mean response, the HS approach offers an alternative way to establishing confidence-like bounds on the expected displacements by varying the auxiliary stiffness \mathbf{C}_0 . In particular, selecting the reference medium such that $\mathbf{C}_0 = \min_i(\mathbf{C}^{(i)})$ yields an upper bound of the stored energy (and therefore the upper “energetic”

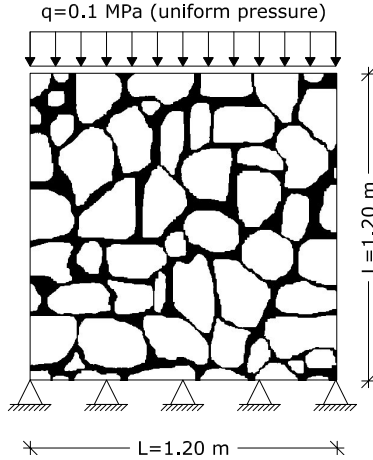


Figure 4: Scheme of an illustrative example

bounds of the displacements), whereas the choice $C_0 = \max_i(C^{(i)})$ results in a lower bound on displacements. Finally, selecting C_0 such that the difference $(C - C_0)$ becomes indefinite provides variational estimates of the basic statistics.

6 Numerical example

In this Section, the essential features of the proposed numerical methods are illustrated by studying elastic response of an irregular masonry structure with dimensions shown in Figure 4 and constant thickness of 0.12 m. The plane stress assumptions were adopted in the analysis; the structure was subject to a uniform pressure applied at the top edge and to the self-weight (a deterministic specific gravity equal to 20 kNm^{-3} was assumed for simplicity). Material constants of individual constituents were considered to be deterministic, the concrete values of the Young moduli $E^{(m)} = 1,200 \text{ MPa}$, $E^{(s)} = 12,500 \text{ MPa}$ and of the Poisson ratios $\nu^{(m)} = 0.3$ and $\nu^{(s)} = 0.2$ were selected following [3]. The geometrical uncertainty due to irregular configuration of individual phases was quantified on the basis of image analysis data presented in Figure 1.

The finite element model of the example problem was based on a regular discretization of the domain using 24×24 square bilinear

elements with four integration points. Note that such a resolution corresponds to the element edge approximately equal to a half of the geometrical correlation length, which is fully consistent with general rules discussed in Sections 3–5.

The results presented for the KLE-based solver were derived from $n = 1,000$ simulations. For simplicity, only the Young modulus E considered in the form of a random field, whereas the Poisson ratio was set to a deterministic value determined from the Voigt estimate of the homogenized stiffness matrix

$$\boldsymbol{\mu}_C = c^{(m)}\mathbf{C}^{(m)} + c^{(s)}\mathbf{C}^{(s)}. \quad (46)$$

Finally, based on a systematic one-dimensional study of the HS approach presented in [16], the element-wise constant discretization of the phase polarization stresses with four-point integration scheme was adopted to ensure sufficient resolution of the spatial statistics.

Before presenting the comparison of individual approaches, we concentrate first on the effect of reference media on the HS-based predictions. To this end, the expected values of nodal displacements are plotted in Figure 5 for several representative choices of \mathbf{C}_0 . In particular, owing to the dominant fraction of the stiffer phase ($c^{(s)} \doteq 67\%$) in the considered structure, the lower energetic bound can be expected to be substantially closer to the “true” statistics than the corresponding upper bound, which in the current case seems to be too inaccurate for practical use. Additional estimates can be generated by the Voigt-type choice (46) or by setting the reference medium to the arithmetic average of properties of individual constituents, the value commonly adopted in the polarization-based numerical method due to Mouline and Suquet [15]. As expected, the response corresponding to such choices is comparable to the lower bound and will be used in the sequel for the comparison with the candidate approaches.

The basic statistics of nodal displacements, as predicted by different methods, are mutually compared in Figure 6. In addition, we present the confidence bounds in the form $\boldsymbol{\mu}_{u_h}(\mathbf{x}) \pm \boldsymbol{\sigma}_{u_h}(\mathbf{x})$, determined on the basis of the second-order statistics for the improved perturbation method (21) or KLE (30). In general, it can be seen that the perturbative method leads to a substantially wider confidence interval when compared to the Monte-Carlo simulation approach, in spite of a moderate number of simulations used by KLE solver to estimate the overall statistics. For both methods, the confidence intervals remain bounded from above by the corresponding HS value. Moreover, for appropriate choices of the reference stiffness matrix, the

HS method recovers the predictions provided by the alternative approaches. For the current setting, selecting C_0 according to the rule of mixtures yields the displacement values almost identical to that of the KLE solver, whereas the response related to the arithmetic average well approximates the improved perturbation result. These results provide just another highlight of the importance of a proper choice of the reference media in the HS-based schemes.

The final comment concerns the computational complexity of individual approaches. It can be stated that the cost of the improved perturbation method and the HS-based solver is roughly comparable, whereas the KLE approach leads to an approximately three-fold increase in the simulation time. Higher cost of the latter method can be attributed to a large number of terms appearing in the expansion (26); the computational cost, however, is compensated by generality of the Monte-Carlo framework and can be further reduced by parallelization of the problem.

7 Conclusions

In this contribution, the applicability of three distinct approaches to mesostructure-based random field simulation of irregular historic masonry was investigated. The numerical results obtained for a finite-size elastic panel allow us to reach the following conclusions:

- The elements of quantification of random spatial statistics can be efficiently used to construct realistic first- and second-order statistics of stationary random fields.
- The improved perturbation method utilizes the second-order statistics when determining the mean response of the system, which generally leads to narrower estimates when compared with the basic method. In the current case, however, the uncertainty in the obtained statistics is higher than for the KLE algorithm, mainly due to a relatively high contrast of phase stiffnesses.
- The Karhunen-Loève series representation coupled with the Monte Carlo approach provides an interesting alternative to the perturbation methods, even at increased computational cost. When applied to realistic structures, however, a large number of terms seems to be necessary to capture the available covariance information. Moreover, the validity of the Gaussian assumption needs to be critically assessed.

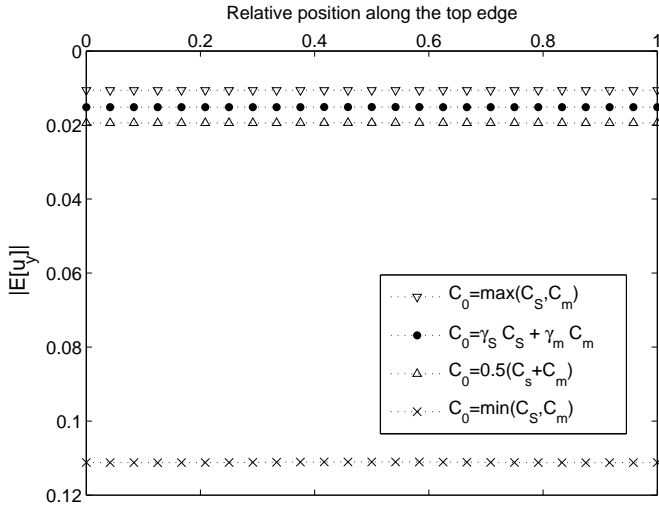


Figure 5: Expected value of nodal displacements via HS-based FE analysis

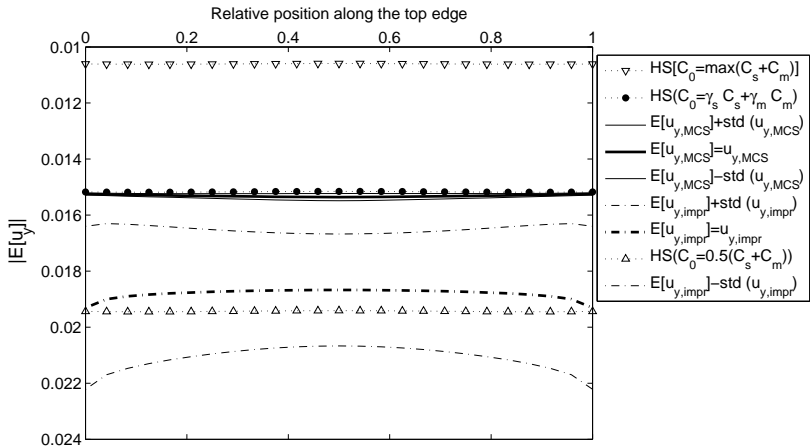


Figure 6: Basic statistics of nodal displacements on the top of the panel

- The Hashin-Shtrikman approach takes advantage of the specific form of the random field and therefore optimally utilizes the available information. The overall response is in this case, however, highly dependent on the choice of the reference medium, for which there is no general rule.

Acknowledgements The support from the Ministry of Education, Youth and Sports, project No. MSM 6840770003 is gratefully acknowledged. Extended form of this lecture can be found in [11].

References

- [1] I. Babuška, R. Tempone, and G. E. Zouraris, *Solving elliptic boundary value problems with uncertain coefficients by the finite element method: the stochastic formulation*, Computer Methods in Applied Mechanics and Engineering **194** (2005), no. 12–16, 1251–1294.
- [2] Z. Bittnar and J. Šejnoha, *Numerical methods in structural mechanics*, ASCE Press and Thomas Telford, Ltd., New York and London, 1996.
- [3] F. Cluni and V. Gusella, *Homogenization of non-periodic masonry structures*, International Journal of Solids and Structures **41** (2004), no. 7, 1911–1923.
- [4] I. Elishakoff, Y. J. Ren, and M. Shinozuka, *Improved finite element method for stochastic problems*, Chaos, Solitons & Fractals **5** (1995), no. 5, 833–846.
- [5] G. Falsone and M. Lombardo, *Stochastic representation of the mechanical properties of irregular masonry structures*, International Journal of Solids and Structures **44** (2007), no. 25–26, 8600–8612.
- [6] J. Gajdošík, J. Zeman, and M. Šejnoha, *Qualitative analysis of fiber composite microstructure: Influence of boundary conditions*, Probabilistic Engineering Mechanics **21** (2006), no. 4, 317–329.
- [7] R. Ghanem and P. D. Spanos, *Stochastic finite elements: A spectral approach*, second revised ed., Dover Publications, Mineola, New York, 2003.
- [8] Z. Hashin and S. Shtrikman, *On some variational principles in anisotropic and nonhomogeneous elasticity*, Journal of the Mechanics and Physics of Solids **10** (1962), 335–342.
- [9] K. Hofstetter, C. Hellmich, and J. Eberhardsteiner, *Development and experimental validation of a continuum micromechanics model for the elasticity of wood*, European Journal of Mechanics A-Solids **24** (2005), no. 6, 1030–1053.
- [10] S. P. Huang, S. T. Quek, and K. K. Phoon, *Convergence study of truncated Karhunen-Loève expansion for simulation of stochastic process*, International

- Journal for Numerical Methods in Engineering **52** (2001), no. 9, 1029–1043.
- [11] M. Lombardo, J. Zeman, M. Šejnoha, and G. Falsone, *Stochastic modeling of chaotic masonry via mesostructural characterization*, 2008, <http://arxiv.org/abs/0811.0972>.
- [12] P.B. Lourenco, G. Milani, A. Tralli, and Zucchini A., *Analysis of masonry structures: Review of and recent trends in homogenization techniques*, Canadian Journal of Civil Engineering **34** (2007), no. 11, 1443–1457.
- [13] R. Luciano and J. R. Willis, *FE analysis of stress and strain fields in finite random composite bodies*, Journal of the Mechanics and Physics of Solids **53** (2005), no. 7, 1505–1522.
- [14] H.G. Matthies, C.E. Brenner, C. G. Bucher, and C. G. Soares, *Uncertainties in probabilistic numerical analysis of structures and solids: Stochastic finite elements*, Structural Safety **19** (1997), no. 3, 283–336.
- [15] H. Moulinec and P. Suquet, *A numerical method for computing the overall response of nonlinear composites with complex microstructure*, Computer Methods in Applied Mechanics and Engineering **157** (1998), no. 1–2, 69–94.
- [16] Z. Sharif-Khodaei and J. Zeman, *Microstructure-based modeling of elastic functionally graded materials: One dimensional case*, Journal of Mechanics of Materials and Structures **3** (2008), no. 9, 1773–1796.
- [17] B. Sudret and A. Der Kiureghian, *Stochastic finite element methods and reliability: A state of the art report*, Tech. Report UCB/SEMM-2000/08, University of California, Berkley, 2000.
- [18] S. Torquato, *Random heterogeneous materials: Microstructure and macroscopic properties*, Springer-Verlag, 2002.
- [19] E. Vanmarke, *Random fields: Analysis and synthesis*, MIT Press, 1998.
- [20] M. Šejnoha and J. Zeman (eds.), *Homogenization in structural engineering applications*, 2009, special issue of International Journal of Multiscale Computational Engineering, to appear.
- [21] V. Šmilauer and Z. Bittnar, *Microstructure-based micromechanical prediction of elastic properties in hydrating cement paste*, Cement and Concrete Research **36** (2006), no. 9, 1708–1718.
- [22] J. R. Willis, *Bounds and self-consistent estimates for the overall properties of anisotropic composites*, Journal of the Mechanics and Physics of Solids **25** (1977), 185–202.
- [23] J. Zeman, J. Novák, M. Šejnoha, and J. Šejnoha, *Pragmatic multi-scale and multi-physics analysis of Charles Bridge in Prague*, Engineering Structures **30** (2008), no. 11, 3365–3376.

Ing. Jan Zeman, Ph.D.

Personal data

Name: Jan Zeman
Born: 19th May 1976
Prague, Czech Republic
Nationality: Czech
E-mail: zemanj@cml.fsv.cvut.cz

Education

2000–2003 Czech Technical University in Prague (Ph.D.)
Klokner Institute
Branch of study: Theory of Structures
1994–2000 Czech Technical University in Prague (Ing.)
Faculty of Civil Engineering
Branch of Study: Building and Structural Engineering
Specialization: Statics of Civil Engineering Structures

Academic experience

2007 Visiting professor
École Normale Supérieure de Cachan, L.M.T. Cachan
2006– Assistant professor
CTU in Prague, Faculty of Civil Engineering
2005–2006 Post-doc researcher (Marie-Curie Fellow)
TU Eindhoven, Mechanics of Materials
2003–2006 Research assistant
CTU in Prague, Faculty of Civil Engineering
2000–2003 Graduate researcher
Czech Technical University in Prague, Klokner Institute
1995–2000 Undergraduate researcher
Czech Technical University in Prague, Klokner Institute

Research activities

Modelling of random composites
Optimization methods
Mathematical modeling of engineering problems
14 publication in ISI Web of Science®
71 citations in ISI Web of Science®
(32 excluding self-citations), *h*-index of 5 (as of 02/01/09).
Principal investigator of 3 grant projects (GAČR, FP7)

Teaching activities

Elastic and Inelastic Analysis of Heterogeneous Materials
Finite Element Method
Loading and Reliability
Modern Optimization Methods
Structural Analysis Techniques
Supervisor of 4 diploma students
(2 awarded the Ivo Babuška Prize)
Co-supervisor and supervisor of 4 Ph.D. students
(2 completed)

Monographs

- [1] M. Šejnoha and J. Zeman, *Micromechanical analysis of random composites*, vol. 6, CTU Reports, no. 1, Czech Technical University in Prague, 2002, 132 pp.
- [2] J. Zeman, *Analysis of composite materials with random microstructure*, vol. 7, CTU Reports, no. 5, Czech Technical University in Prague, 2003, 177 pp.

ISI Web of Science journal publications (2007–2008)

- [1] M. Šejnoha, J. Šejnoha, M. Kalousková, and J. Zeman, *Stochastic analysis of failure of earth structures*, *Probabilistic Engineering Mechanics* **22** (2007), no. 2, 206–218.
- [2] J. Zeman and M. Šejnoha, *From random microstructures to representative volume elements*, *Modelling and Simulation in Materials Science and Engineering* **15** (2007), no. 4, S325–S335.
- [3] M. Šejnoha and J. Zeman, *Micromechanical modeling of imperfect textile composites*, *International Journal of Engineering Science* **46** (2008), no. 6, 513–526, (Special issue: Micromechanics of Materials).
- [4] B. Tomková, M. Šejnoha, J. Novák, and J. Zeman, *Evaluation of effective thermal conductivities of porous textile composites*, *International Journal for Multiscale Computational Engineering* **6** (2008), no. 2, 153–167.
- [5] J. Šejnoha, M. Šejnoha, J. Zeman, J. Sýkora, and J. Vorel, *A mesoscopic study on historic masonry*, *Structural Engineering & Mechanics* **30** (2008), no. 1, 99–117.
- [6] J. Skoček, J. Zeman, and M. Šejnoha, *Effective properties of textile composites: Application of the Mori-Tanaka method*, *Modelling and Simulation in Materials Science and Engineering* **16** (2008), no. 8, 085002 (15pp).
- [7] J. Zeman, J. Novák, M. Šejnoha, and J. Šejnoha, *Pragmatic multi-scale and multi-physics analysis of Charles Bridge in Prague*, *Engineering Structures* **30** (2008), no. 11, 3365–3376.
- [8] Z. Sharif-Khodaei and J. Zeman, *Microstructure-based modeling of elastic functionally graded materials: One dimensional case*, *Journal of Mechanics of Materials and Structures* **3** (2008), no. 9, 1773–1796.